Interplay of strain and magnetism in $La_{1-x}Sr_xMnO_3$ from first principles

Giuseppe Colizzi, Alessio Filippetti, Fabrizio Cossu, and Vincenzo Fiorentini
Dipartimento di Fisica and INFM-SLACS, Università di Cagliari, I-09042 Monserrato (Ca), Italy
(Received 29 July 2008; revised manuscript received 11 November 2008; published 22 December 2008)

The structural, electronic, and magnetic properties of $La_{0.625}Sr_{0.375}MnO_3$ under planar and orthogonal (i.e., uniaxial) strains are investigated from first-principles generalized gradient approximation (GGA) and GGA $+U$ approaches. We analyze a series of magnetic phase transitions from ferromagnetic to *A*-type and *C*-type antiferromagnetic orderings caused by uniaxial strain at various in-plane lattice constants. The competition between ferromagnetic and antiferromagnetic interactions obeys the following general rule: antiferromagnetic coupling is enhanced in the direction parallel to applied strain, while ferromagnetic coupling is enhanced in the orthogonal direction. The microscopic mechanisms at the basis of the strain effects are analyzed in detail.

DOI: 10.1103/PhysRevB.78.235122 PACS number(s): 71.15.Mb, 75.47.Lx, 71.20.−b, 75.25.+z

I. INTRODUCTION

An exciting frontier for spintronic applications is the field of magnetic multilayered heterostructures and thin-film devices capable of cleverly exploiting magnetoelectric, magnetoelastic, and magnetoresistive effects. Candidate building blocks for this technology are manganese perovskite [e.g., $La_{1-x}Sr_xMnO_3$ (LSMO)] films, with their unique variety of magnetic and magnetostrictive properties.[1–10] Potentially revolutionary functionalities of manganite-based heterostructures are, to quote but a few, large magnetorestivity in LSMO-sandwiched carbon nanotube,[11] magnetotransport in $LSMO/BaTiO_3$ and $LSMO/SrTiO_3$ multilayers,[12,13] magnetoelectric effects in LSMO/piezoelectric and LSMO/ferroelectric interfaces,[14,15] and proximity effects in ferromagnetic (FM)/superconducting heterostructures.[16]

For many of these capabilities, a preponderant role is assumed by the strain. Understanding how structural, magnetic, and transport properties are affected, and can be eventually controlled, by the applied strain is instrumental to elucidate the fundamental coupling mechanisms and to trace design rules for devices with improved performances. A formidable deal of experimental work has been carried out to investigate strain effects in either bulk or thin-film manganites,[17–21] Experiments have emphasized the crucial role of strain in a range of fundamental aspects of manganite (especially LSMO) films: metal-insulating phase coexistence,[22] phase separation,[23] orbital reconstruction,[24,25] formation of magnetic stripe domains,[26,27] inhomogeneities,[28,29] electronic transport,[30,31] anomalies in magnetostriction, and thermal expansion.[32]

On the theoretical side, studies treating equilibrium bulk properties abound;[10,33–35] strain effects are less studied, either by model calculations[31,36,37] or first-principles approaches.[10,38–41] Structural distortions in tetragonal LSMO are extensively treated in Refs. 38 and 39 but limited to FM order, whereas in the seminal work by Fang *et al.*[10] the magnetic phase competition as a function of the orthogonal/planar lattice ratio (c/a) is investigated by GGA calculations. There, the general behaviors of magnetization under strain have been identified and interpreted coherently with many experimental findings. Nevertheless, a complete understanding of the massive experimental data for manganite films is far from accomplished.

Usually, strain effects are understood in terms of bandwidth and hopping parameter changes, in turn linked to the magnetic interactions according to the prescription of double-exchange (DE) model. In this framework a compressive strain is usually associated with the enhancement of T_C and FM coupling,[36] whereas tensile strain is thought to suppress FM double-exchange and reduce conductivity.[26,42–44] However, these behaviors are not univocally reproduced, and opposite trends have been reported as well.[45–49] In many studies on the subject, a key assumption is that the dependence on the tetragonal distortion c/a captures the whole dependence on strain. In fact, manganite properties can be sensitive to the separate action of in-plane (substrate-induced) strain and out-of-plane uniaxial strain.

In the present paper we give a comprehensive analysis of uniaxial and in-plane strain effects on structural, electronic, and magnetic properties in tetragonal LSMO. We choose the Sr concentration $x=0.375$, safely in the FM metallic region. Our focus is on the competition between FM and several antiferromagnetic (AF) order patterns. We recently reported in Ref. 41 a similar study of rhombohedral LSMO under *hydrostatic* pressure. In this paper, instead, structural parameters are chosen to mimic pseudomorphic growth conditions on noncompliant substrates. We consider three values of in-plane lattice constant (a) corresponding to planar strains ranging from strongly compressive (−5.2%) to weakly tensile (1.2%).[17,18] The lattice-constant values correspond to the three widely used substrates $YAlO_3$, $LaAlO_3$, and $SrTiO_3$. In the following, we will often refer to our in-plane lattice-constant change as a substrate-induced strain. For each such strain, LSMO properties are evaluated in a wide range of orthogonal strain (c/a from 0.95 to 1.15), with full atomic relaxation at each (a,c) configuration. In this way the action of planar and vertical strains is disentangled, and a complete picture of tetragonal LSMO under generic strain is obtained.

In our calculations we employed two different approaches: the generalized gradient approximation (GGA) and the GGA$+U$.[50] It is important, for a reliable description, to carry out studies with both methods in parallel. Although GGA is accurate enough for optimally doped LSMO, electron correlation effects are still important for specific properties (such as, e.g., magnetic moments and density of states, as will be shown below) and especially for large applied strains, which can severely change the density of states at

Fermi energy (E_F) and, hence, the degree of electron correlation (i.e., localization) in the system.

Overall, magnetic ordering in LSMO turns out to be quite sensitive to applied strain and, hence, potentially suited for, e.g., piezomagnetic applications. It will be shown that the system response in terms of structural distortions [e.g., Jahn-Teller (JT)] and change in magnetization is highly anisotropic. Under uniaxial strain, the FM phase (stable at the equilibrium) is disrupted in favor of either *A*-type or *C*-type AF coupling, depending on whether compressive or tensile strain is applied. This behavior was already pointed out in previous theoretical works,[10] but here we show that the choice of different substrates can remarkably alter the magnetic phase competition. In fact, two independent strain parameters enable nice tunability of the magnetic properties as they respond to the external strain in highly anisotropic fashion. Compression favors FM-AF switch but only in the direction parallel to the applied strain while it strengthens the FM coupling orthogonally to the strain. In this way one may stabilize AF_A-type ordering through the *c* axis (e.g., mechanical) compression or AF_C-type ordering by substrate shrinking.

It is also known that the anisotropic strain can dramatically alter the electronic properties of the manganites and even turn LSMO in insulator.[20,30,31,51] This may in principle be due to different (possibly coupled) sources: atomic displacements and change in magnetic coupling. With our analysis of the electronic properties we rationalize the microscopic mechanisms governing conduction properties under strain and the respective influences of structural distortions and magnetic phase competition.

The work is organized as follows. In Sec. II we give technical details about the calculations. In Sec. III we discuss results concerning total energies (Sec. III A), structural parameters (Sec. III B), and electronic properties (Sec. III C). Section IV is devoted to comment and discuss our results, and finally in Sec. V we offer our conclusions.

II. METHODS

First-principles calculations are performed using the projector augmented wave (PAW) method[52] as implemented in the Vienna *ab initio* simulation package (VASP) code.[53] As energy functionals we used standard GGA and GGA+U [50] (U is the on-site Coulomb repulsion included for the Mn *d* electrons) in the Dudarev implementation.[54] We set $U=3$ eV and the exchange interaction $J=0.98$ eV [as in our previous work on rhombohedral LSMO (Ref. 41)]. An energy cutoff of 300 eV and a $4\times4\times4$ Monkhorst-Pack *k*-point grid are adopted. All calculations are done within $2\times2\times2$ (40 atom) cubic supercells which are sufficient to simulate bulk LSMO in $R\bar{3}c$ rhombohedral symmetry at low temperature. Doping at $x=0.375$ concentration is treated with Sr substitutions on La sites, chosen according to the calculated lowest-energy configuration at equilibrium (i.e., at vanishing stress). For each structure (i.e., applied strain) full atomic relaxation is performed.

We considered four magnetic-order arrangements: FM, *C*-type antiferromagnetic with spin wave vector $\mathbf{q}=[1/2,1/2,0]$ (AF_C), and two *A*-type antiferromagnetic orderings corresponding to $\mathbf{q}=[0,0,1/2]$ (AF_A^z) and $\mathbf{q}=[1/2,0,0]$ (AF_A^x). Notice that the last two are not identical under planar or vertical applied strain.

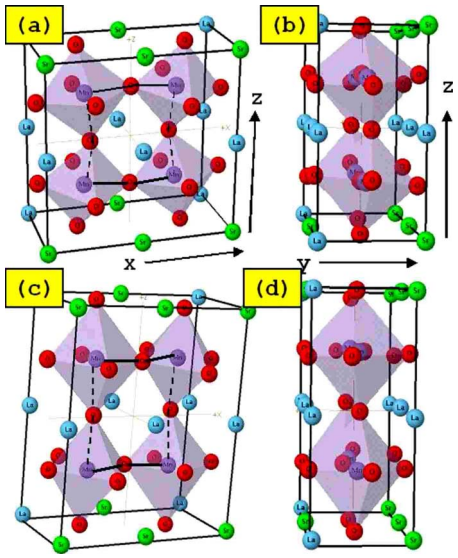

FIG. 1. (Color online) Calculated structure of tetragonal LSMO under strain at $a=3.80$ Å. (a) and (b): three-dimensional and side view for $c/a=0.95$ (i.e., under strong out-of-plane compressive strain). (c) and (d): same perspectives for $c/a=1.15$, that is, strong orthogonal tensile strain. Solid and dashed lines draw planar and out-of-plane Mn-O-Mn angles, respectively.

Calculations are done for three in-plane lattice constants: $a=3.95$, 3.80, and 3.70 Å. As our theoretical lattice constant for rhombohedral LSMO is $a_0=3.905$ Å,[41] the chosen lattice constants correspond to planar strains $\epsilon_a\sim1.1\%$, -2.6%, and -5.2%, which approximately correspond to the experimental growth conditions on $SrTiO_3$, $LaAlO_3$, and $YAlO_3$ substrates, respectively. Sketches of the structure for the $LaAlO_3$-epitaxial condition at two c/a values are displayed in Fig. 1.

III. RESULTS

A. Energies and magnetic ordering under strain

In this section we discuss the energetics of LSMO and the competition among magnetic orderings as a function of epitaxial substrate (i.e., a) and orthogonal strain (c/a). We start in Fig. 2 with the GGA-calculated total energies as a function of a and c/a. The curves relative to different substrates are well distinguishable, and for each substrate the minimal energy corresponds to a well-defined c/a value largely independent of the specific magnetic order. This implies that a change in magnetic order (e.g., by application of a magnetic field) should not cause substantial changes in the structure. We will see that the reverse does not hold; that is, a suitable strain does in fact change the magnetic ordering.

Let us analyze the energy curves for each substrate. At $a=3.95$ Å the minimum $c/a=0.98$ is close to unity as expected, with the FM ordering visibly favored, in accord with observations. Moving along the curve toward larger c/a the

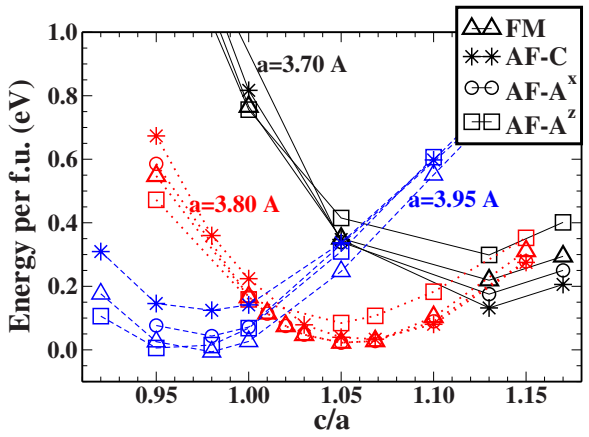

FIG. 2. (Color online) GGA-calculated total energies per formula unit versus the ratio c/a for different a and magnetic orderings.

FM phase remains favored, with the various AF orderings gaining some stability. More interestingly, at $c/a \sim 0.96-0.97$ (that is, for small compressive longitudinal strain $\epsilon_c \sim -1$ and -2%) we find an energy crossing between AF_A^z and FM, with the former becoming more and more stable along with the progressive shrinking of the orthogonal axis. At $c/a=0.92$ the AF_A^z has already a sizable energetic advantage over the FM ($\Delta E=-70.3$ meV/formula unit); thus, a sign change in the orthogonal exchange interaction is prospected. The AF_A^z stability is further strengthened by an in-plane compression: we see that for fixed c/a, smaller a lowers the AF_A^z energy even more with respect to the FM: at $c/a=0.95$, $\Delta E=-20.2$, -75.2, and -89.9 meV/f.u. for $a=3.95$, 3.80, and 3.70 Å, respectively. See also Table I where energies for all the considered magnetic phases are reported at selected structural parameters and corresponding strain values.

Consider now the energy curves for $a=3.80$ Å, they all have minima at $c/a \sim 1.05$ (i.e., $c=3.99$ Å); i.e., not surprisingly a compressive planar strain induces a substantial stretching in the orthogonal direction. This sensitively alters the magnetic phase competition: at equilibrium the FM phase is nearly degenerate with the AF_A^x and is favored by 16.8 meV/f.u. over the AF_C and by 61.6 meV over the AF_A^z. However, a relatively small change in c/a is sufficient to reverse the order: for $c/a \sim 1.08$ (corresponding to a tensile strain $\epsilon_c \sim 2-3\%$), it makes the AF_C favored and stable at any larger c. Orthogonal compression, instead, favors the AF_A^z ordering, similar to the previously discussed case of $a=3.95$ Å.

Finally, for $a=3.70$ Å LSMO properties depart even more dramatically from the equilibrium: the energy minimum at $c/a=1.13$ corresponds to a remarkable orthogonal elongation ($c=4.181$ Å). Here the AF_C phase is largely favored and remains stable under compression of up to $c/a \sim 1.05$. Between $c/a=1.05$ and 1.0 another crossing shows up, and the AF_A^z phase (the highest in energy for c/a above

TABLE I. GGA-calculated total energies (in meV/f.u.) of LSMO in several magnetic orderings for different substrates (a) and out-of-plane strain (c/a). For each a and c energies are referred to the most stable magnetic phase. The corresponding planar (ϵ_a) and orthogonal (ϵ_c) strains, and the c-axis component of the stress tensor (in GPa) averaged over different magnetic phases at each strain are also reported. Positive and negative stress values refer to compressive and tensile stresses, respectively.

c/a		σ_{zz}	FM	AF_C	AF_A^x	AF_A^z
$a=3.95$ Å	$\epsilon_a=1.1\%$					
0.95	$\epsilon_c=-3\%$	5.6	20	140	71	0
1.0	$\epsilon_c=+2\%$	−7.9	0	115	58	42
1.05	$\epsilon_c=+5\%$	−15.3	0	90	30	63
1.1	$\epsilon_c=+10\%$	−16.1	33	80	0	89
1.15	$\epsilon_c=+15\%$	−16.5	69	107	0	126
$a=3.80$ Å	$\epsilon_{xy}=-2.6\%$					
0.95	$\epsilon_c=-9\%$	32.0	75	201	113	0
1.0	$\epsilon_c=-5\%$	12.8	7	65	9	0
1.05	$\epsilon_c=0$	−0.1	0	17	0	62
1.1	$\epsilon_c=+5\%$	−10.6	23	0	9	102
1.15	$\epsilon_c=+9\%$	−14.3	36	0	3	77
$a=3.70$ Å	$\epsilon_{xy}=-5.2\%$					
0.95	$\epsilon_c=-16\%$	58.9	90	155	97	0
1.0	$\epsilon_c=-11\%$	32.7	9	61	10	0
1.05	$\epsilon_c=-7\%$	16.1	12	8	0	76
1.13	$\epsilon_c=0\%$	−3.3	87	0	43	166
1.17	$\epsilon_c=+3\%$	−10.3	88	0	44	195

1.05) suddenly takes place and remains stable at any lower c/a.

The results just seen suggest some well-defined tendencies. First, in-plane shrinking (i.e., smaller lattice-constant substrate) makes LSMO stretch orthogonally (provided it is left unconstrained along c) and reach equilibrium at $c=3.87$, 3.99, and 4.18 Å for $a=3.95$, 3.80, and 3.70 Å, respectively. The in-plane shrinking and its complementary c elongation alter magnetic ordering, favoring the stabilization of the AF_C phase over the FM. Notice that even for tensile in-plane strain ($a=3.95$ Å), although never stable in our examined c/a range, the AF_C gains substantial energy with increasing c, with respect to all other orderings. On the other hand, if for a fixed substrate the c axis is suitably shrunk, we can induce further phase transitions in the system: from FM to AF_A^z for $a=3.95$ Å; from AF_C to FM and then to AF_A^Z for $a=3.80$ Å; and from AF_C to AF_A^z for $a=3.70$ Å.

In Table I we report the calculated internal stress tensor component σ_{zz} at the various vertical strains ϵ_c. Apart from a sign change, this is the pressure that should be applied along the c axis in order to produce that strain. In the calculation, of course, the strain is simply imposed geometrically on the supercell. It can be noticed that the pressure values in question are fairly large but reachable in an anvil cell and possibly also in a piezodevice setting.

The general tendency toward AF_C or AF_A^z stabilization upon c/a increase or decrease, respectively, was first described by *ab initio* calculations in Ref. 10, where a universal diagram as a function of doping concentration x and c/a was drawn.[23] Our results on the one hand confirm this picture but on the other attest that the c/a dependence is not really universal but crucially depends on specific c and a values. Thus, intriguingly, the control of the c-axis length by external pressure may be a straightforward way to manipulate the magnetic ordering of the system. Over the years, a number of experimental works (typical resistivity and magnetization measurements)[18,51] have confirmed that applied strain can indeed dramatically alter conducting and magnetic properties of the systems in a sense that is compatible with the theoretical results, although no direct proof of a phase transition has been furnished, to our knowledge.

It is appropriate to check the GGA results with GGA+U. In Fig. 3 our GGA+U-calculated energies are shown in the same format used in Fig. 2. Despite minor quantitative differences, the picture drawn by GGA calculations is substantially confirmed: the AF_C phase is still favored (although in a smaller c/a range) with respect to the FM by the c-axis elongation, while the AF_A^z is stable for any substrate upon the c-axis shrinking. As for the equilibrium structures, equilibrium is reached at $c/a=0.98$, 1.07, and 1.13 for $a=3.95$, 3.80, and 3.70 Å, respectively; thus, values are substantially equal to those obtained within GGA. Given this similarity in the energetics representation, the analysis of structural properties under strain in Sec. III B will be limited to the GGA results only.

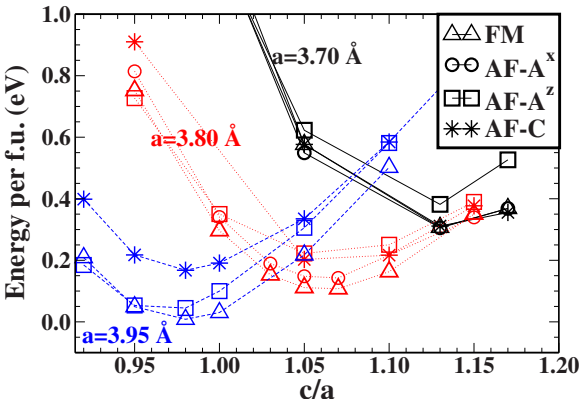

FIG. 3. (Color online) GGA+U total energies per formula unit versus the ratio c/a for different a and magnetic orderings.

B. Structural changes under strain

Understanding the competition among magnetic phases requires a comparative analysis of the structural changes under applied strain. For perovskites, the fundamental structural degrees of freedom are Mn-O distances and Mn-O-Mn angles which are easily related to octahedral rotations (sketched in Fig. 1). These quantities can be conveniently expressed through averages of in-plane and out-of-plane angles. In Table II we report for each substrate the GGA-calculated equilibrium values of c, and planar (labeled with x) and vertical (z) Mn-O-Mn angles and Mn-O distances. As these structural parameters are barely sensitive to the specific magnetic order (in consistency with the total-energy results) the values in the table are averaged over the considered magnetic phases.

We start with the analysis of in-plane angles, as reported in Fig. 4. At each fixed substrate, we see that moving from large to small c/a causes a smooth, regular increase in the angles (i.e., decrease in octahedral rotations) up to $c/a\sim 1$. Below this threshold a plateau is reached. This behavior fol-

TABLE II. GGA-calculated equilibrium structural parameters for each fixed substrate. Parameters include the c-axis length (in Å), average in-plane (θ_a) and out-of plane (θ_c) Mn-O-Mn angles, in-plane $(\text{Mn-O})_a$ and out-of-plane $(\text{Mn-O})_c$ distances (in Å), and Jahn-Teller distortion, calculated as $(\text{Mn-O})_c$ and $(\text{Mn-O})_a$ differences relative to their mean value. All values are averaged over the magnetic orderings as structure dependence on the specific ordering is minimal and can be discarded.

a	c	c/a	θ_a	θ_c	$(\text{Mn-O})_a$	$(\text{Mn-O})_c$	JT
3.95	3.87	0.98	168°	162°	1.98	1.95	−0.015
3.80	4.07	1.07	158°	178°	1.91	2.02	+0.056
3.70	4.18	1.13	155°	178°	1.88	2.10	+0.110

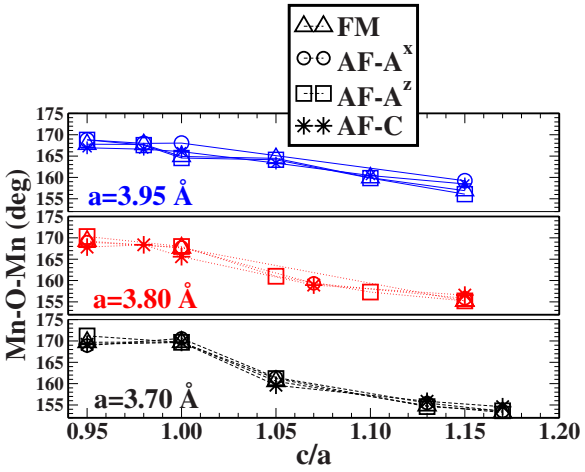

FIG. 4. (Color online) Cell-averaged, in-plane Mn-O-Mn angles versus ratio c/a, as calculated in GGA. Each panel reports values for a given in-plane lattice constant a and several magnetic orders.

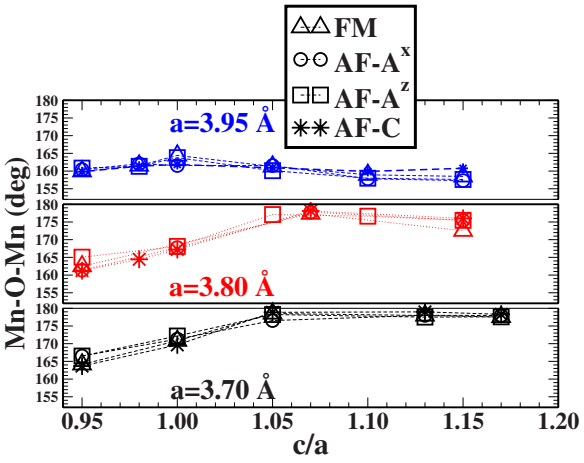

FIG. 5. (Color online) Cell-averaged, out-of-plane Mn-O-Mn angles versus ratio c/a calculated within GGA. Each panel refers to a given in-plane lattice constant a and several magnetic orders.

lows the usual space-filling argument, according to which oxygen rotations take place in order to shorten their distance from A-site cations, while shrinking c flatten angles in the (x,y) plane orthogonal to the applied strain direction. This directionality is fundamental to understand the different behaviors of in- and out-of-plane angles and can be visually appreciated in Fig. 1 comparing panels (b) (short c) and (d) (long c): we see that in-plane rotations increase with c in such a way that oxygens get closer to two of their four A-site nearest neighbors stretched apart by the c-axis elongation.

On the other hand, if we keep c/a fixed (i.e., scales a and c simultaneously), the angles are much less responsive to applied strain: fixing, e.g., $c/a=1$ and moving from larger to smaller substrates, angles decrease (i.e., rotation increases) in accord to the space-filling criterion, from $\sim 170°$ at $a=3.70$ Å to $\sim 165°$ at $a=3.95$ Å (the $c/a=1$ case corresponds to the hydrostatic strain studied in detail in Ref. 41). This indicates that a nonisotropic applied strain is far more effective than the hydrostatic strain in stimulating large structural response.

The out-of-plane angle behavior under applied strain is shown in Fig. 5. Here for each substrate we can distinguish two regimes: at large c/a angles are nearly constant with c/a. In this region, for compressive planar strain ($\epsilon_a<0$) angles are close to 180°; i.e., octahedra are almost completely stretched out along the c axis. Then a cusp shows up at $c/a\sim 1.05$ below which angles rapidly fall; i.e., oxygens rotate around the c axis. (Notice that for consistency at $c/a=1$ in-plane and out-of-plane angles coherently converge to the same values.) For the tensile substrate $a=3.95$ Å at large c/a vertical angles are much smaller than for compressive substrates (i.e., oxygens rotate more in accord with the space-filling argument) and remain nearly constant through the whole c/a range, although the cusp is still visible at $c/a\sim 1$.

In summary, in the small c/a regime vertical angles do not follow the space-filling rule anymore, as they fall consistently along with c/a. This can be explained in terms of the Mn-O repulsion coming into play when their distance becomes too short. Mn-O distances are reported in Fig. 6, also separated in in-plane (upper panel) and out-of-plane (lower panel) contributions. In the plane, the $(\text{Mn-O})_a$ distances are obviously dependent on the substrate but weakly dependent on c, and they remain close to the respective equilibrium values (see Table II) through the whole c/a range. No regime change is triggered. On the contrary, $(\text{Mn-O})_c$ distances are highly responsive to change in c, and moving through the c/a range, they shrink by as much as $\sim 20\%$ their equilibrium length. At $c/a=1$, for example, our calculations give $(\text{Mn-O})_z=1.95$, 1.90, and 1.85 Å for $a=3.95$, 3.80 and 3.70 Å substrates, respectively, corresponding to Mn-O strained by $\epsilon=0$, -6%, and -12% with respect to their equilibrium values (see Table II). Strong repulsive strain activates c-axis oxygen rotations (i.e., smaller $(\text{Mn-O-Mn})_z$ angle) allowing some Mn-O elongation [the minimum value $(\text{Mn-O})_z=c/2$ corresponds to $(\text{Mn-O-Mn})_z=180°$].

Finally, not surprisingly, as we move to more and more compressive substrates, Jahn-Teller distortions consistently show up. They are quantified in Table II as relative difference between in-plane and out-of-plane average Mn-O distances.

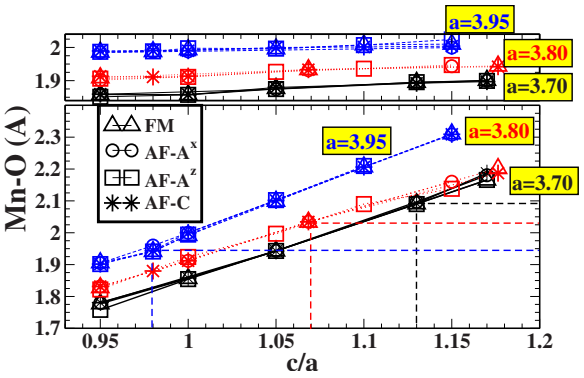

FIG. 6. (Color online) Top: GGA-calculated average Mn-O distances parallel to the x and y planes as a function of c/a for each substrate and magnetic orderings. Bottom: same as top but for vertical Mn-O distances. For each substrate dashed lines highlight equilibrium c and corresponding Mn-O values.

With the analysis of structural changes in the hands, we can go back to the energy results and give a straightforward interpretation of the magnetic phase competitions: Stretching c produces large in-plane rotations and nearly vertical octahedral alignment; this strengthens the AF_C stability over all the other magnetic phases, in coherence with the usual picture according to which FM double-exchange interactions are enhanced by flatter Mn-O-Mn angles (thus larger p-d hybridization). According to Fig. 2, a FM-AF_C crossing takes place at large c/a for the two compressive substrates but not for $a=3.95$ Å, and now we understand why: for the latter substrate in-plane rotations are not large enough to reverse the magnetic interactions.

On the other hand, shortening c favors the AF_A^z stabilization as vertical angles get smaller and planar angles stretch out. The mechanism of FM-AF_A^z crossing is arguably quite robust as it occurs at any substrate and is equally predicted by GGA and GGA+U results. This aspect is the main highlight of our study as far as interest in design applications is concerned.

C. Electronic properties

Electronic properties and the orbital-resolved density of states (OR-DOS) give us the microscopic keys to uncover the mechanism driving the system response to applied strain. To emphasize the vertical (i.e., uniaxial) strain effects, we juxtapose the OR-DOS calculated at the end-points range ($c/a=0.95$ and 1.15), limiting the discussion to the most important magnetic orderings, i.e., FM, AF_A^z (stabilized under vertical compression), and AF_C (stabilized by vertical tensile strain). The main characteristics of the OR-DOS and the conclusions of our analysis do not depend on the specific substrate, so we only discuss results for one intermediate case. Thus it is understood that all pictures shown below are for $a=3.80$ Å and either $c/a=0.95$ or $c/a=1.15$.

Usually for manganese perovskites the density of states (DOS) and magnetic moments are particularly sensitive to computational technicalities, as a small difference in spin-splitting energy can sensitively alter the orbital occupations on which magnetic moments crucially depends, at variance with total energies and structural properties, which are only marginally affected by the use of either GGA or GGA+U. In our previous work on bulk rhombohedral LSMO,[41] we found that GGA sizably underestimates the spin-splitting energy, and an applied compressive strain may therefore induce a sharp drop of Mn magnetic moments due to the shift of unoccupied Mn e_g minority bands below the Fermi energy (E_F). A similar behavior may be arguably expected even for nonisotropic compression.

In Figs. 7 and 8 we report the OR-DOS calculated in GGA and GGA+U for the FM phase under vertical compression. Indeed, the difference is especially apparent for the Mn: in GGA the spin-polarized t_{2g} orbitals are split by only ~2.2 eV. Compressive strain further squeezes these orbitals which spread out in space to reduce their electrostatic repulsion, thus reducing even more the associated spin splitting. In GGA at $c/a=0.95$ the bottom of minority t_{2g} bands lies below E_F and the respective DOS is partially filled. This

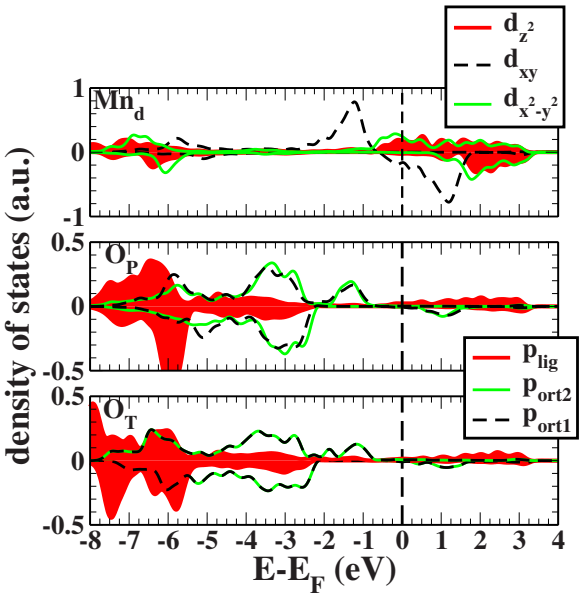

FIG. 7. (Color online) Orbital-resolved DOS for Mn and O atoms in the FM phase calculated within GGA at planar lattice constant $a=3.80$ Å and $c/a=0.95$ (i.e., under vertical compression). O_P and O_T refer to in-plane and on-top oxygens, respectively; p_{lig} is the ligand orbitals directed to the Mn (i.e., p_z for O_P and either p_x or p_y for O_T); and p_{ort1} and p_{ort2} are the two nonligand orbitals directed orthogonally to the Mn-O bond.

makes magnetic moments strongly sensitive to a change in c/a. In GGA+U the spin splitting of the t_{2g} orbitals is remarkably larger (~4 eV) so that minority t_{2g} remain well above E_F even under strong longitudinal compression and magnetic moments do not degrade. As for magnetic moments, the GGA and GGA+U differences are relatively mi-

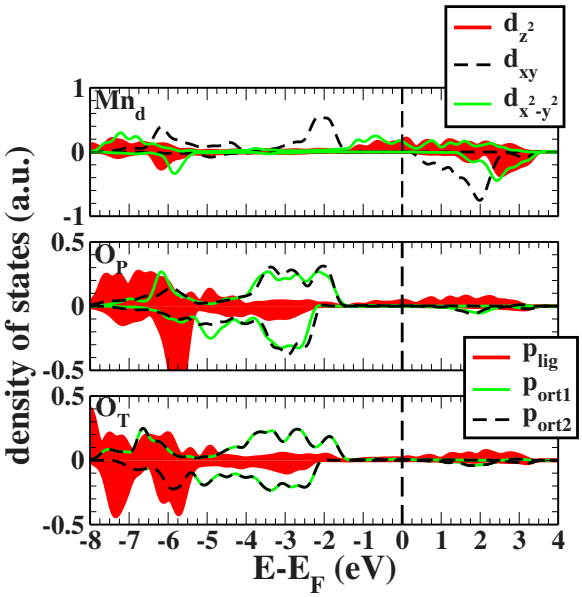

FIG. 8. (Color online) Orbital-resolved DOS for Mn and O atoms in the FM phase calculated within GGA+U at $a=3.80$ Å and $c/a=0.95$ (vertical compression). Labels are described in the caption of Fig. 7.

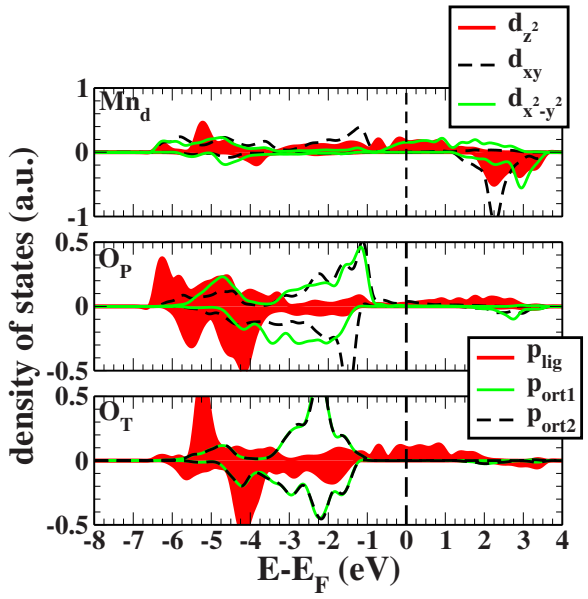

FIG. 9. (Color online) Orbital-resolved DOS for Mn and O atoms in the FM phase calculated within GGA+U at a=3.80 Å and c/a ratio of c/a=1.15 (vertical stretching). Labels are described in the caption of Fig. 7.

nor at a=3.95 Å (at equilibrium c/a=0.98 we have, averaging over different phases, $M=\sim 3.4\mu_B$ in GGA+U and $\sim 3.2\mu_B$ in GGA), while for a=3.80 Å GGA+U gives M $\sim$3.2–3.4 Å, while GGA $\sim$3.0–3.2 Å. Since we can safely assume the GGA+U description as the correct one, in what follows we concentrate our analysis on the GGA+U results only.

Comparing the FM DOS in Fig. 8 with that in Fig. 9, corresponding to c/a=1.15, we see that the c-axis compression causes a large spread of valence bandwidth (from $\sim$7 eV at c/a=1.15 to $\sim$8 eV at c/a=0.95) associated with a remarkable charge delocalization. Furthermore, c/a=0.95 is a condition of weak anisotropy (i.e., not too far from c/a=1) so the ligand DOS of on-top oxygen (p_z) and in-plane oxygen (either p_x or p_y) are similar (Fig. 8), with $p_{\rm lig}$ partially filled and spin antialigned to the Mn, furnishing a small negative contribution to the magnetic moment. Looking at the orbital occupations for the FM phase in Table III, at c/a=0.95 we have $M_{\rm Mn}=3.29\mu_B$, of which $2.51\mu_B$ come from t_{2g}, $0.45\mu_B$, and $0.33\mu_B$ from x^2-y^2 and z^2, respectively. Also $p_{\rm lig}$ contributes with $\sim -0.06\mu_B$, but this is overcompensated by a positive $p_{\rm ort}$ contribution of $\sim 0.1\mu_B$, so the total magnetization per formula unit (Mn plus O_T plus two O_P) is $M=3.40\mu_B$.

At c/a=1.15 the structure is much more anisotropic, with nearly flat vertical angles and large octahedral rotations in the plane. This is reflected in the difference between O_P and O_T ligand DOS in Fig. 9: for O_P, the $p_{\rm lig}$ DOS tail crossed by E_F is thinner under tension, as a consequence of the accentuated planar rotations, while the same orbital for O_T is enhanced due to the realignment of the octahedra along c. We can see in Table III that stretching c/a from 0.95 to 1.15, x^2-y^2 and z^2 occupations change by −0.15 and +0.04 electrons, respectively, and O_T $p_{\rm lig}$ by −0.14 electrons. In words, elongation causes an enhancement of the p-d hybridization (evidenced by the charge transfer from O_T $p_{\rm lig}$ to Mn z^2) in the orthogonal Mn-O bonds and a decrease in p-d hybridization (charge loss in Mn x^2-y^2 orbital) in planar Mn-O bonds. As for magnetic moments, at c/a=1.15 we have $M_{\rm Mn}$ $=3.45\mu_B$ ($2.53\mu_B$ from t_{2g} and $0.33\mu_B$ and $0.59\mu_B$ from x^2-y^2 and z^2, respectively), $0.01\mu_B$ from O_P and $-0.03\mu_B$ from O_T, for a total $M=3.44\mu_B$ per formula unit.

On the basis of this picture, and according to the usual arguments of superexchange (SE) theory, we can conclude that vertical elongation causes the enhancement of ferromagnetic coupling in the direction of the applied strain (i.e., along c) and antiferromagnetic coupling in the plane (i.e., orthogonally to the applied strain). This picture is coherent, indeed, with our total-energy calculations, which indicate a strengthening of AF_C ordering at large c/a.

Let us now consider the DOS of the AF_A^z phase under compression (Fig. 10). The AF_A^z symmetry takes advantage of the longitudinal compression, as small in-plane rotations (Mn-O-Mn $\sim$ 170°) and large out-of-plane rotations (Mn-O-Mn $\sim$ 162°) strengthen planar FM coupling and longitudinal AF coupling, respectively. With respect to the more isotropic FM ordering, the two e_g orbitals present a more marked difference, with x^2-y^2 DOS more occupied than z^2; i.e., with respect to the FM ordering a portion of e_g charge is transferred from the vertical axis to the plane. This anisotropy is also reflected in the oxygens: the $p_{\rm lig}$ DOS around E_F is visibly larger for O_P than for O_T. Notice also that while O_P is spin-polarized due to double-exchange interactions with Mn, O_T is nonmagnetic due to the vertical AF symmetry.

Under vertical tension the situation is reversed: vertical angles (Mn-O-Mn $\sim$ 175°) are straightened, and in-plane angles (Mn-O-Mn $\sim$ 155°) are sharpened. Although the AF_A^z order is now disfavored, it is interesting to see how the DOS, in Fig. 11, reacts in order to minimize the disadvantage due to the stretching: the Mn e_g's are completely pulled apart, with majority z^2 almost completely filled (its band top lying approximately half eV below E_F) similar to the t_{2g} (see the corresponding occupation in Table III) and the x^2-y^2 DOS largely depleted and cut by E_F at the bottom. The Mn z^2 is strongly coupled with majority O_T $p_{\rm lig}$ which also lies well below E_F and is completely filled. As a consequence, O_T $p_{\rm lig}$ is no longer spin compensated as it was under pressure and contributes with additional $0.06\mu_B$ to the total moment.

The magnetization of O_T $p_{\rm lig}$ seems to be at odds with the AF_A^z symmetry, which should favor nonmagnetic oxygens. The inspection of atomic relaxations reveals that O_T's go substantially off center with respect to the two spin-antipaired nearest Mn aligned along z and get closer to one of those to form a succession of $\sim$1.9–2.0 Å long Mn-O dimers separated by $\sim$2.3–2.4 Å distance. The dimers are characterized by the strong $p_z^{\uparrow}$-$d_{z^2}^{\downarrow}$ coupling, as revealed by the DOS analysis, so that each dimer forms a magnetic polaron of $\sim 3.55\mu_B$. The dimerization is associated with a buckling in the MnO_2 planes and to polar displacements neutralized in overall antiferroelectric fashion.

Finally we come to the AF_C phase, stable at large orthogonal stretching. See first the OR-DOS under compression in Fig. 12. The rationale of DOS variations upon applied

TABLE III. Orbital occupations calculated within GGA+U at a=3.80 Å and c/a=0.95 and 1.15 for FM, AF_A^z, and AF_C orderings.

	FM		AF_A^z		AF_C	
c/a	0.95	1.15	0.95	1.15	0.95	1.15
			Mn			
$d^{\uparrow}_{x^2-y^2}$	0.70	0.57	0.72	0.55	0.81	0.52
$d^{\downarrow}_{x^2-y^2}$	0.25	0.24	0.25	0.23	0.21	0.25
$d^{\uparrow}_{z^2}$	0.61	0.76	0.56	0.93	0.62	0.80
$d^{\downarrow}_{z^2}$	0.28	0.17	0.30	0.11	0.26	0.17
$d^{\uparrow}_{xy}$	0.95	0.90	0.95	0.90	0.93	0.90
$d^{\downarrow}_{xy}$	0.10	0.11	0.10	0.11	0.09	0.12
$d^{\uparrow}_{xz}$	0.94	0.94	0.93	0.94	0.94	0.94
$d^{\downarrow}_{xz}$	0.11	0.07	0.12	0.06	0.10	0.08
M_{Mn} (μ_B)	3.29	3.45	3.20	3.69	3.48	3.40
			O_P			
$p^{\uparrow}_{\mathrm{lig}}$	0.68	0.66	0.68	0.65	0.72	0.70
$p^{\downarrow}_{\mathrm{lig}}$	0.74	0.73	0.74	0.73	0.72	0.70
$p^{\uparrow}_{\mathrm{ort1}}$	0.78	0.76	0.78	0.76	0.75	0.75
$p^{\downarrow}_{\mathrm{ort1}}$	0.73	0.73	0.73	0.73	0.76	0.75
$p^{\uparrow}_{\mathrm{ort2}}$	0.79	0.76	0.78	0.76	0.76	0.73
$p^{\downarrow}_{\mathrm{ort2}}$	0.74	0.71	0.74	0.71	0.76	0.73
M_{O_P} (μ_B)	0.04	0.01	0.03	0	−0.01	0
			O_T			
$p^{\uparrow}_{\mathrm{lig}}$	0.71	0.63	0.74	0.72	0.70	0.66
$p^{\downarrow}_{\mathrm{lig}}$	0.76	0.70	0.74	0.66	0.77	0.70
$p^{\uparrow}_{\mathrm{ort1}}$	0.78	0.75	0.76	0.73	0.78	0.74
$p^{\downarrow}_{\mathrm{ort1}}$	0.74	0.73	0.76	0.74	0.74	0.73
$p^{\uparrow}_{\mathrm{ort2}}$	0.78	0.75	0.76	0.73	0.78	0.74
$p^{\downarrow}_{\mathrm{ort2}}$	0.74	0.73	0.76	0.74	0.74	0.73
M_{O_T} (μ_B)	0.03	−0.03	0	0.04	−0.01	−0.02
M_{tot} (μ_B)	3.40	3.44	3.26	3.73	3.45	3.38

strain is reversed with respect to the AF_A^z phase, as now spins are longitudinally aligned and planar antialigned. Under compression the O_T DOS nearby E_F is depressed, as a sign of the reduced Mn-O_T hybridization due to the increased octahedral tilting, while a sizable Mn-O_P hybridization is still present. Now in-plane AF and out-of-plane FM couplings are clearly disfavored by this trend. On the contrary, tensile strain (Fig. 13) reverts the situation, thus Mn-O_T d_{z^2}-p_{lig} hybridization is visibly amplified at E_F, while Mn-O_P $d_{x^2-y^2}$-p_{lig} coupling is switched off, as much as the planar DOS is almost gapped (with just a tail of $d_{x^2-y^2}$ DOS peak cut by E_F).

In summary, our GGA+U description of the OR-DOS is coherent with previous experimental and theoretical reports which indicate an imbalance in the two e_g orbitals due to the applied strain,[10,23,25] causing charge filling of z^2 or x^2-y^2 depending on whether an in-plane (x,y) or uniaxial (z-parallel) compression is applied. However, the amount of charge imbalance can also vary according to the magnetic ordering; thus its effect on the conduction properties depends on which magnetic ordering is stable at the considered strain.

IV. DISCUSSION

On the basis of our results for tetragonal LSMO we can trace a coherent description of LSMO properties under strain. Starting with structural properties, we have previously found in Ref. 41 that, in agreement with observations, hydrostatic compression reduces oxygen rotations, decreases Mn-O distances, and favors a more cubiclike, undistorted symmetry.[55] For nonisotropic strain this prescription still holds but must be suitably generalized: according to the space-filling argument, oxygens strive to shorten the distance from the A-site cation. Then, a unidirectional lattice elongation along, e.g., the z axis, increases the O-A distance within the (x,z) and (y,z) planes but leaves unchanged the same distance within the (x,y) plane orthogonal to the strain di-

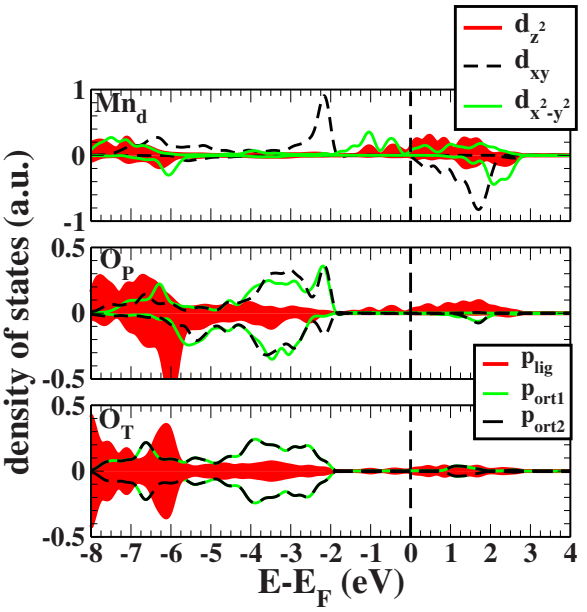

FIG. 10. (Color online) Orbital-resolved DOS for Mn and O atoms in the AF_A^z phase calculated within GGA+U at a=3.80 Å under orthogonal compressive strain (c/a=0.95).

rection so that only octahedral rotations parallel to (x,y) are stimulated. That is, stretching induces rotations in the plane orthogonal, but not parallel, to the applied strain direction. This is a key concept to understand the whole structural response of LSMO to an applied unidirectional strain: for fixed substrate, stretching c causes in-plane angle decrease, i.e., larger oxygen rotations (Fig. 4), while vertical angles remain nearly constant (Fig. 5) for c values above a minimal threshold. Shrinking c below this threshold, vertical Mn-O bonds (Fig. 6) become repulsive and the vertical octahedra rotate to relieve the pressure. This happens, in our calculations, at a

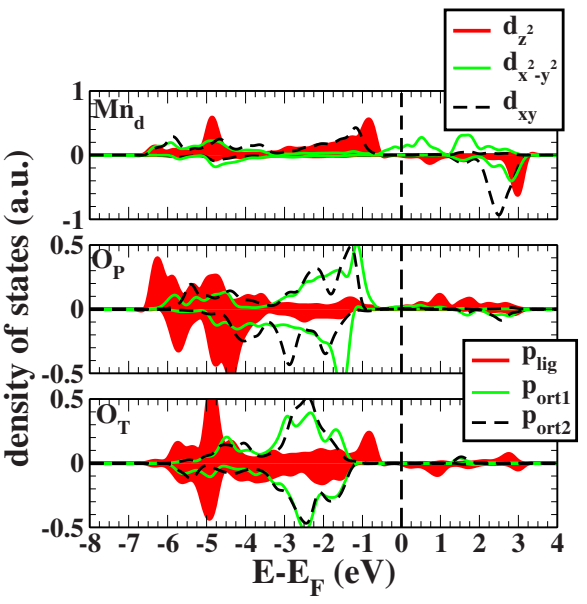

FIG. 11. (Color online) Orbital-resolved DOS for Mn and O in the AF_A^z phase calculated within GGA+U at a=3.80 Å under orthogonal tensile strain (c/a=1.15).

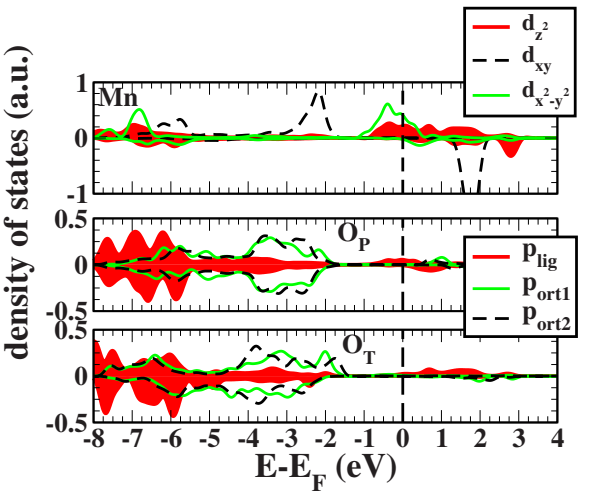

FIG. 12. (Color online) OR-DOS for Mn and O atoms in the AF_C phase calculated within GGA+U at a=3.80 Å and orthogonal compression c/a=0.95.

pressure of approximately 20 GPa. A similar abrupt reduction in the vertical Mn-O-Mn angle at high pressure was observed also in other manganite systems as, for example, the orthorhombic $La_{0.60}Y_{0.07}Ca_{0.33}MnO_3$ crystals under high hydrostatic pressure.[56]

Structural distortions are instrumental in understanding magnetic phase stability competition under strain. In agreement with experiments, the FM phase is found stable at equilibrium (i.e., zero pressure) against several AF phases considered here (Fig. 2). However, this competition is highly sensitive to the application of unidirectional strain. Uniaxial compression favors the enhancement of AF and FM couplings along and orthogonally to the strain direction, respectively, favored by larger longitudinal and smaller in-plane oxygen rotations. The situation is completely reversed for uniaxial elongation as now FM and AF coupling are strengthened along and orthogonally to the strain direction, respectively, to flatter vertical and sharper in-plane octahedral angles.

This behavior has a simple interpretation in terms of double-exchange interactions, as illustrated by the calculated

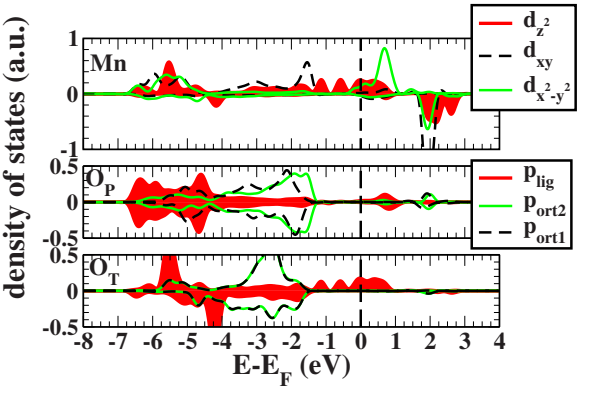

FIG. 13. (Color online) OR-DOS for Mn and O atoms in the AF_C phase calculated within GGA+U at a=3.80 Å and orthogonal tension c/a=1/15.

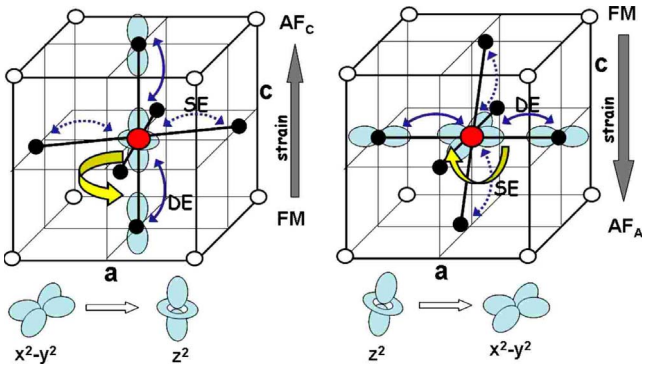

FIG. 14. (Color online) Schematic effects of uniaxial strain on LSMO [indicated by thick (gray) vertical arrows]. [Mn: large (red) circles; O: small filled circles; and La/Sr: small empty circles.] The applied strain is indicated by thick (gray) vertical arrows. Left panel: vertical elongation. Right panel: vertical compression. Curled (yellow) arrows show corresponding octahedral rotations, i.e., in-plane for elongation and out-of-plane for compression. The directions of prevailing DE and SE interactions are highlighted by thin (blue) Mn-O connecting arrows (solid for DE and dashed for SE). The corresponding charge transfer between the relevant Mn orbitals involved in the process is also showed at the bottom.

DOS under compressive and tensile uniaxial strains: compression favors flat angles and larger *p-d* hybridization around E_F in the plane, tilted octahedra, and less *p-d* hybridization longitudinally. It is very clear from the DOS calculated under uniaxial compression (compare the DOS for FM in Fig. 8, AF_A^z in Fig. 10, and AF_C in Fig. 12) that the only *p-d* hybridization (i.e., p_{lig}-$d_{x^2-y^2}$ overlap) near E_F comes from Mn-O_P bonds, while the Mn-O_T d_{z^2}-p_{lig} contribution is swept off. The enhancement of planar FM double-exchange and vertical AF superexchange follows. Under tensile strain the situation is reversed as the Mn-O_T d_{z^2}-p_{lig} hybridization is now always predominant over the Mn-O_P $d_{x^2-y^2}$-p_{lig} counterpart (see Fig. 9, Fig. 11, and Fig. 13 for FM, AF_A^z, and AF_C, respectively); thus, we can expect stronger FM double-exchange longitudinally and AF superexchange in the plane. As a summary, in order to convey an immediate feeling of the essential response of magnetic and structural properties to uniaxial strain, we have drawn in Fig. 14 a schematic picture linking uniaxial strain with orbital charge transfer, octahedral rotations, and corresponding magnetic interactions strengthened by the applied strain.

This general picture of magnetization under uniaxial strain is qualitatively valid at any examined substrate, but the choice of the substrate largely influences the practical possibility to induce a phase transition in the system. As a general rule, the larger the planar strain imposed by the substrate, the larger the orthogonal response of the systems (i.e., the Jahn-Teller distortion) and then the possibility to destabilize the equilibrium FM ordering. The highly compressive substrates studied here favor large vertical elongation; thus, they have a fundamental role in the stabilization of the AF_C phase under uniaxial elongation. In Table I we have seen that the AF_C is never stable at $a=3.95$ Å; it can be stable at $a=3.80$ Å only upon application of a considerable ($\epsilon_c=5\%$) tensile strain, and it is finally stable at $a=3.70$ Å at equilibrium c (i.e., $\epsilon_c=0$). Thus, the only practical way of stabilizing AF_C is, according to our results, growing on very compressive substrates. (Consistently with our present results, as we will report elsewhere, AF_C order is also locally stabilized at the Mn-terminated surface of LSMO with $a=3.80$ Å, i.e., grown on $LaAlO_3$.)

On the other hand, turning on AF_A^z order appears more likely since, looking again at Table I, it can be stabilized at any substrate provided that a sufficient compressive strain is applied longitudinally. The required strain is very large at $a=3.70$ Å ($\epsilon_c=-11\%$) but seems plausible for $a=3.80$ Å ($\epsilon_c=-5\%$) and $a=3.95$ Å ($\epsilon_c=-3\%$).

It is worth mentioning that GGA results found that the AF_A may be stabilized even by isotropic (i.e., hydrostatic) compressive strain $\epsilon\sim-2-3\%$.[10,41] However this result is in contrast with GGA+U, which confirms the FM stability even up to extremely high pressure. For uniaxial compression this ambiguity does not appear as GGA (Fig. 2) and GGA+U (Fig. 3) delineate a substantially equivalent picture of the magnetic phase competitions. The role of structural anisotropy in the FM-to-AF_A transition was previously suggested for other manganites with orthorhombic symmetry [e.g., $La_{1-x}Ca_xMnO_3$ and $Pr_{1-x}Sr_xMnO_3$ (Ref. 21)].

Finally, within GGA+U the calculated magnetization is essentially constant under hydrostatic pressure (in agreement with experiments[57]) or under planar strain provided that the equilibrium c for each substrate is maintained (in agreement with the findings reported in Ref. 39). This seems to conflict with magnetization measurements of FM LSMO films grown on various substrates.[9,12,14,18] This disagreement between *ab initio* calculations and experiments may be either due to surface effects, not considered in the present calculations, or more likely to the possible coexistence of FM and AF (and/or spin-glass) phases.[9]

V. CONCLUSIONS

We have investigated structural, magnetic, and electronic properties of tetragonal LSMO under condition of in-plane (e.g., substrate-induced) and uniaxial (c-parallel) strains using first-principles GGA and GGA+U approaches. We have described the general behavior of magnetic properties under strain and provided a straightforward interpretation of the relation between structural changes, electronic properties, and magnetic ordering competition. Uniaxial stretching along c produces large in-plane rotations, longitudinal octahedral alignment (i.e., flatter vertical angles), and enhancement of vertical *p-d* hybridization. The latter strengthens the AF_C stability over all the other competing orderings, coherently with the usual FM double-exchange picture, and determines the FM-AF_C crossing at large c/a for the two examined compressive substrates (except for the tensile $a=3.95$ Å as in the latter in-plane rotations are not large enough to reverse the magnetic interactions). These results emphasize the separate role played by the substrate and uniaxial strains and question the interpretation of the strain dependence in terms of the c/a ratio only. On the other hand, shortening c favors the AF_A^z stabilization as vertical angles become smaller and planar angles stretch out. The mecha-

nism of FM-AF^z_A crossing is arguably robust as it occurs at any substrate and is equally predicted by GGA and GGA $+U$ results.

In conclusion, magnetization in LSMO appears to respond very sensitively and anisotropically to either planar or uniaxial strain, suggesting some simple ideas for tuning magnetic ordering in designed applications. However, a better assessment of the LSMO films properties and more reliable comparison with the observations will require the simulations of actual multilayers, e.g., LSMO layers interfaced by substrate and vacuum on the two sides, as the presence of surfaces and interfaces probably plays an important role in the magnetic properties physics of manganite films.

ACKNOWLEDGMENTS

A.F. thanks MIUR project "Cervelli per la ricerca" for early financial support. Work was supported in part by MIUR through PON-CyberSar project and PRIN05, and by Fondazione Banco di Sardegna. Calculations were performed on the Cybersar@UNICA and SLACS-HPC@CASPUR clusters.

[1] S. Jin, T. H. Tiefel, M. McCormack, R. A. Fastnacht, R. Ramesh, and L. H. Chen, Science **264**, 413 (1994).
[2] M. Yoshimoto, H. Maruta, T. Ohnishi, K. Sasaki, and H. Koinuma, Appl. Phys. Lett. **73**, 187 (1998).
[3] L. Zhang, C. Isreael, A. Biswas, R. L. Greene, and A. de Lozanne, Science **298**, 805 (2002).
[4] S. Mercone, C. A. Perroni, V. Cataudella, G. De Filippis, C. Adamo, M. Angeloni, C. Aruta, F. Miletto-Granozio, A. Oropallo, P. Perna, A. Yu. Petrov, U. Scotti di Uccio, G. Balestrino, and L. Maritato, J. Supercond. **18**, 119 (2005).
[5] M. Mathews, F. M. Postma, J. Cock Lodder, R. Jansen, G. Rijnders, and D. H. A. Blank, Appl. Phys. Lett. **87**, 242507 (2005).
[6] I. Pallecchi, L. Pellegrino, E. Bellingeri, A. S. Siri, and D. Marré, Phys. Rev. B **71**, 014406 (2005).
[7] A. A. Sidorenko, G. Allodi, R. De Renzi, G. Balestrino, and M. Angeloni, Phys. Rev. B **73**, 054406 (2006).
[8] T. Taniuchi, H. Kumigashira, M. Oshima, T. Wakita, T. Yokoya, M. Kubota, and K. Ono, Appl. Phys. Lett. **89**, 112505 (2006).
[9] A. Geddo Lehmann, C. Sanna, N. Lampis, F. Congiu, G. Concas, L. Maritato, C. Aruta, and A. Yu. Petrov, Eur. Phys. J. B **55**, 337 (2007).
[10] Z. Fang, I. V. Solovyev, and K. Terakura, Phys. Rev. Lett. **84**, 3169 (2000).
[11] L. E. Hueso, J. M. Proneda, V. Ferrari, G. Burnell, J. P. Valdés-Herrera, B. D. Simons, P. B. Littlewood, E. Artacho, A. Fert, and N. D. Mathur, Nature (London) **445**, 410 (2007).
[12] Y. P. Lee, S. Y. Park, Y. H. Hyun, J. B. Kim, V. G. Prokhorov, V. A. Komashko, and V. L. Svetchnikov, Phys. Rev. B **73**, 224413 (2006).
[13] L. M. Wang, Jing-Kae Lin, and Jong-Pyng Shyu, Phys. Rev. B **74**, 184412 (2006).
[14] C. Thiele, K. Dorr, O. Bilani, J. Rodel, and L. Schultz, Phys. Rev. B **75**, 054408 (2007).
[15] R. K. Zheng, Y. Wang, H. L. W. Chan, C. L. Choy, and H. S. Luo, Phys. Rev. B **75**, 212102 (2007).
[16] A. I. Buzdin, Rev. Mod. Phys. **77**, 935 (2005).
[17] Y. Konishi, M. Kasai, M. Izumi, M. Kawasaki, and Y. Tokura, Mater. Sci. Eng., B **56**, pp. 158–163(6) (1998).
[18] F. Tsui, M. C. Smoak, T. K. Nath, and C. B. Eom, Appl. Phys. Lett. **76**, 2421 (2000).
[19] A. Chikamatsu, H. Wadati, H. Kumigashira, M. Oshima, A. Fujimori, N. Hamada, T. Ohnishi, M. Lippmaa, K. Ono, M. Kawasaki, and H. Koinuma, Phys. Rev. B **73**, 195105 (2006).
[20] S. Jin, G. Gao, W. Wu, and X. Zhou, J. Phys. D **40**, 305 (2007).
[21] D. P. Kozlenko and B. N. Savenko, Phys. Part. Nucl. **37**, S1 (2006).
[22] K. H. Ahn, T. Lookman, and A. R. Bishop, Nature (London) **428**, 402 (2004).
[23] A. Tebano, C. Aruta, P. G. Medaglia, F. Tozzi, G. Balestrino, A. A. Sidorenko, G. Allodi, R. De Renzi, G. Ghiringhelli, C. Dallera, L. Braicovich, and N. B. Brookes, Phys. Rev. B **74**, 245116 (2006).
[24] C. Aruta, G. Ghiringhelli, A. Tebano, N. G. Boggio, N. B. Brookes, P. G. Medaglia, and G. Balestrino, Phys. Rev. B **73**, 235121 (2006).
[25] A. Tebano, C. Aruta, S. Sanna, P. G. Medaglia, G. Balestrino, A. A. Sidorenko, R. De Renzi, G. Ghiringhelli, L. Braicovich, V. Bisogni, and N. B. Brookes, Phys. Rev. Lett. **100**, 137401 (2008).
[26] J. Dho, Y. N. Kim, Y. S. Hwang, J. C. Kim, and N. H. Hur, Appl. Phys. Lett. **82**, 1434 (2003).
[27] J. Dho, N. H. Hur, I. S. Kim, and Y. K. Park, J. Appl. Phys. **94**, 7670 (2003).
[28] R. Di Capua, C. A. Perroni, V. Cataudella, F. Miletto Granozio, P. Perna, M. Salluzzo, U. Scotti di Uccio, and R. Vaglio, J. Phys.: Condens. Mat. **18**, 8195 (2006).
[29] G. Gao, S. Jin, and W. Wu, Appl. Phys. Lett. **90**, 012509 (2007).
[30] X. J. Chen, S. Soltan, H. Zhang, and H.-U. Habermeier, Phys. Rev. B **65**, 174402 (2002).
[31] P. Dey, T. K. Nath, and A. Taraphder, Appl. Phys. Lett. **91**, 012511 (2007)
[32] L. I. Koroleva and R. V. Demin, Physica B **259**, 816 (1999).
[33] D. J. Singh and W. E. Pickett, Phys. Rev. B **57**, 88 (1998).
[34] G. Banach and W. M. Temmerman, Phys. Rev. B **69**, 054427 (2004).
[35] V. Ferrari, J. M. Pruneda, and E. Artacho, Phys. Status Solidi A **203**, 1437 (2006).
[36] A. J. Millis, T. Darling, and A. Migliori, J. Appl. Phys. **83**, 1588 (1998).
[37] C. A. Perroni, V. Cataudella, G. De Filippis, G. Iadonisi, V. Marigliano Ramaglia, and F. Ventriglia, Phys. Rev. B **68**, 224424 (2003).
[38] T. Geng and N. Zhang, Phys. Lett. A **351**, 314 (2006).
[39] C. Ma, Z. Yang, and S. Picozzi, J. Phys.: Condens. Matter **18**, 7717 (2006).
[40] M. Talati and P. K. Jha, Phys. Rev. B **74**, 134406 (2006).
[41] G. Colizzi, A. Filippetti, and V. Fiorentini, Phys. Rev. B **76**,

064428 (2007).
[42] B. Vengalis, A. Maneikis, F. Anisimovas, R. Butukuté, L. Dapkus, and A. Kindurys, J. Magn. Magn. Mater. **211**, 35 (2000).
[43] F. S. Razavi, G. Gross, H.-U. Habermeier, O. Lebedev, S. Amelincks, G. Van Tendeloo, and A. Vigliante, Appl. Phys. Lett. **76**, 155 (2000).
[44] S. I. Khartsev, P. Johnsson, and A. M. Grishin, J. Appl. Phys. **87**, 2394 (2000).
[45] G. Q. Gong, A. Gupta, G. Xiao, P. Lecoeur, and T. R. McGuire, Phys. Rev. B **54**, R3742 (1996).
[46] R. A. Rao, D. Lavric, T. K. Nath, C. B. Eom, L. Wu, and F. Tsui, J. Appl. Phys. **85**, 4794 (1999).
[47] W. Prellier, A. M. Hagiri-Gosnet, B. Mercey, Ph. Lecoeur, M. Hervieu, Ch. Simon, and B. Raveau, Appl. Phys. Lett. **77**, 1023 (2000).
[48] J. Zhang, H. Tanaka, T. Kanki, J.-H. Choi, and T. Kawai, Phys. Rev. B **64**, 184404 (2001).
[49] S. S. Dhesi, G. van der Laan, E. Dudzik, and A. B. Shick, Phys. Rev. Lett. **87**, 067201 (2001).
[50] V. I. Anisimov, J. Zaanen, and O. K. Andersen, Phys. Rev. B **44**, 943 (1991).
[51] Y. Takamura, R. V. Chopdekar, E. Arenholz, and Y. Suzuki, Appl. Phys. Lett. **92**, 162504 (2008).
[52] P. E. Blöchl, Phys. Rev. B **50**, 17953 (1994).
[53] G. Kresse and J. Furthmüller, Comput. Mater. Sci. **6**, 15 (1996); Phys. Rev. B **54**, 11169 (1996); G. Kresse and D. Joubert, *ibid.* **59**, 1758 (1999).
[54] S. L. Dudarev, G. A. Botton, S. Y. Savrasov, C. J. Humphreys, and A. P. Sutton, Phys. Rev. B **57**, 1505 (1998).
[55] Y. Morimoto, A. Asamitsu, and Y. Tokura, Phys. Rev. B **51**, 16491 (1995).
[56] C. Cui, T. A. Tyson, Z. Zhong, J. P. Carlo, and Y. Qin, Phys. Rev. B **67**, 104107 (2003).
[57] D. P. Kozlenko, I. N. Goncharenko, B. N. Savenko, and V. I. Voronin, J. Phys.: Condens. Matter **16**, 6755 (2004).